Numerical Ellipsometry Analysis (NEA) of Nanoscale Gold Gratings

Chao Zeng[1,2], Shayesteh Raeisi[1,3], Szanto Geza[1], Jeetendra Gour[4], Thomas Siefke[4,5,6], Miklós Fried[1,2], Péter Petrik*[1,3]

1. Centre for Energy Research, Institute of Technical Physics & Materials Science, Konkoly-Thege Rd. 29-33,1121 Budapest, Hungary.

2. Doctoral School on Materials Sciences and Technologies, Óbuda University, 1034 Budapest, Hungary.

3. Department of Electrical Engineering, Institute of Physics, Faculty of Science and Technology, University of Debrecen, Bem tér 18, Debrecen, 4026, Hungary.

4. Friedrich Schiller University Jena, Institute of Applied Physics, Jena, Germany

5. Fraunhofer IOF, Jena, Germany

6. University of Applied Sciences, Jena, Germany

Corresponding author: Miklos Fried, fried.miklos@kvk.uni-obuda.hu, Péter Petrik, petrik.peter@ek.hun-ren.hu

Abstract: This study presents a comprehensive numerical ellipsometry analysis of gold nanograting by integrating an advanced simulation platform, COMSOL Multiphysics. The proposed hybrid approach enables detailed investigation of the optical properties and polarization-dependent responses of plasmonic nanostructures. Simulations were conducted for various incident angles (Φ = 60°, 65°, 70°, and 75°) and grating periods (CD = 70 and 110 nm) to evaluate the influence of structural parameters on the ellipsometry spectra. The simulated results show a good agreement with experimental ellipsometry measurements obtained from fabricated nanograting, leaving room for further improvement of the combined method. This work demonstrates that the integration of numerical ellipsometry modeling with finite-element and finite-element–frequency-domain solvers provide a powerful and efficient tool for the design and optimization of high-sensitivity optical and plasmonic sensors.

Keywords: Numerical ellipsometry, Gold nanograting, ellipsometry spectra, plasma resonance

1. Introuduction

Diffraction gratings are fundamental optical components that play a crucial role in manipulating and controlling light propagation [1]. Their periodic micro- or nanostructures introduce spatial modulation of the amplitude or phase of incident electromagnetic waves, resulting in the diffraction of light into multiple directions according to wavelength [2]. This wavelength-dependent diffraction enables gratings to perform spectral dispersion, making them indispensable in both fundamental research and practical optical systems. Owing to their unique optical and structural characteristics, diffraction gratings have been widely utilized in a broad range of applications, including optical coupling, spectral filtering, optical communication, laser engineering, thin-film stabilization, photodetection, solar energy concentration, and spectroscopic analysis[3].

In recent years, the study of metallic gratings has opened a new research frontier in the field of diffractive and plasmonic optics [4]. Unlike dielectric gratings, metallic gratings exhibit distinctive optical properties arising from the excitation of surface plasmon polaritons (SPPs)—collective oscillations of free electrons at the metal–dielectric interface that couple with incident electromagnetic waves [4, 5]. These plasmonic resonances enable strong light–matter interactions and electromagnetic field confinement beyond the diffraction limit, providing novel mechanisms for manipulating light at the nanoscale [6]. As a result, metallic gratings have attracted significant attention from researchers worldwide and have found extensive applications in areas such as plasmon-enhanced lithography, near-field optical microscopy, light extraction and modulation in light-emitting diodes (LEDs), and high-sensitivity photodetection [7]. Furthermore, their ability to enhance local electromagnetic fields and improve light coupling efficiency has demonstrated great potential in industrial sensing, military optical systems, and biomedical diagnostics, establishing metallic gratings as key elements in the development of next-generation photonic and optoelectronic technologies.

Despite the extensive research on diffraction and plasmonic phenomena in metallic gratings, accurately describing and predicting their optical responses remain challenging due to the complex coupling between incident electromagnetic waves and surface plasmon modes. The optical behavior of such structures is highly sensitive to factors such as the grating period, groove depth, duty cycle, dielectric environment, and the intrinsic dielectric function of the metallic material. Traditional analytical approaches, while offering physical insight, are often insufficient for quantitatively reproducing experimental results, especially in nanostructured systems exhibiting strong near-field interactions and non-linear effects [8].

To solve these challenges, this work aims to establish a comprehensive numerical and experimental framework for investigating the optical characteristics of metallic gratings. The primary objectives are: (1) to model and analyze the plasmonic and diffractive responses of metallic gratings using advanced electromagnetic simulation tools such as COMSOL Multiphysics; (2) to characterize their optical constants and structural parameters through spectroscopic ellipsometry; and (3) to correlate simulation results with experimental measurements for validating physical models and optimizing design parameters. Through this integrated approach, the work seeks to deepen the understanding of light–matter interactions in periodic metallic nanostructures and to provide theoretical and experimental support for their application in high-performance photonic and sensing devices [9].

2. Sample preparation and numerical simulation environment

2.1 Sample preparation

The fabrication of nanostructured metallic gratings typically involves a sequence of high-precision micro–nanofabrication processes designed to achieve periodic metallic patterns with subwavelength dimensions. These structures are crucial for manipulating light–matter interactions at the nanoscale, particularly for applications in plasmonics, sensing, and photonic devices [10, 11]. In this work, periodic gold gratings were fabricated using a top-down approach based on electron beam lithography (EBL). This technique was chosen to achieve the high pattern fidelity required by the designed structure. The main fabrication process of the gold gratings is illustrated in Fig. 1, process began with an optical-grade fused silica substrate, onto which a Cr/Au/Cr layer was sequentially deposited to provide adhesion, a functional gold layer, and a chromium hard mask for subsequent pattern transfer. The desired grating pattern was defined in the resist layer using electron-beam lithography (EBL), followed by resist development to form high-resolution nanoscale features. The pattern was first transferred into the top Cr hard mask using ion beam etching (IBE). Afterward, the remaining resist was completely removed by oxygen plasma ashing to prevent contamination and ensure accurate pattern definition. The grating pattern was then transferred from the Cr mask into the underlying Au layer via reactive ion beam etching (RIBE), achieving anisotropic sidewalls and precise dimensional control through a combination of physical sputtering and chemical etching mechanisms. Finally, the residual Cr hard mask was removed using inductively coupled plasma (ICP) etching, resulting in the final periodic gold grating structure.

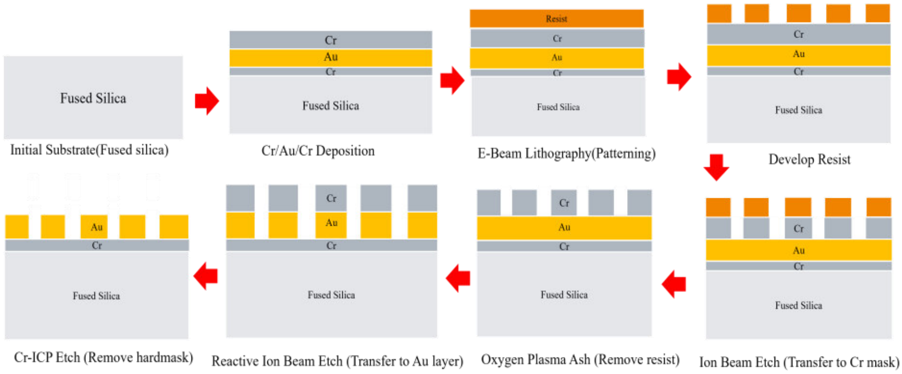

Figure1.Schematic of the fabrication steps for Au nanograting

Periodic gold gratings (period Λ =200 nm) were patterned on glass substrates by electron-beam lithography. Gold films of thickness (dg =60 nm) were deposited by magnetron sputtering and patterned by lift-off, yielding line widths (CD) of 70, 90, 110 and 130 nm, as shown in Fig. 2.

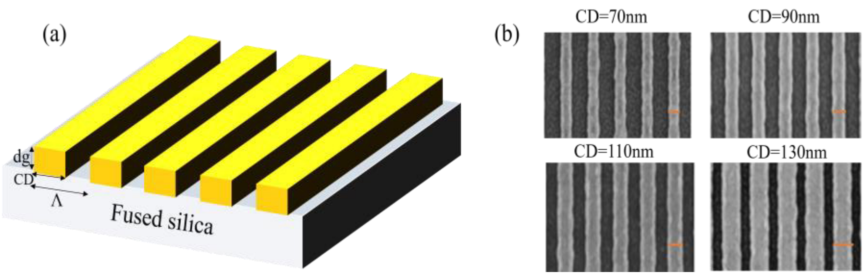

Figure 2. (a) Schematic and (b) SEM images of Au gratings fabricated on fused silica substrate

2.2 Numerical simulation environment

In this simulation, the Wave Optics Module of COMSOL Multiphysics was used to simulate light propagation through diffraction gratings. The optical response was defined using S-parameters obtained from the “Electromagnetic Waves, Frequency Domain” interface [12, 13]. The simulation is based on Rigorous Coupled-Wave Analysis (RCWA). In this model, an electromagnetic plane wave is incident from the air region onto the sample, and the light interacting with the structured surface is collected from both the substrate and the superstrate. And we can get key optical parameters including reflectance (R), transmittance (T), the Brewster angle, and the electric-field distribution can be extracted. These quantities are obtained by solving the frequency domain partial differential equations (1.1) governing the electric and magnetic fields (E and H) during wave propagation through the structure.

$$\nabla \times \mu_r^{-1}(\nabla \times E) - \omega^2 \varepsilon_0 \mu_0 (\varepsilon_r - i\sigma / \omega\varepsilon_0)E = 0 \qquad (1.1)$$

Here, μ_r is the relative permeability, ε_0 is the vacuum permittivity, μ_0 is the vacuum permeability, ε_r is the relative permittivity, and σ is the electrical conductivity.

To model TE (s-polarization) and TM (p-polarization) polarized illumination in a two-dimensional layout, the field vectors must be assigned in accordance with the incidence plane (xy). In COMSOL Multiphysics, s-polarization is imposed by defining the electric field exclusively along the out-of-plane axis (E = (0, 0, 1)). In contrast, p-polarization is implemented using the in-plane wave-vector formulation, where the magnetic field is oriented normal to the computational plane (H = (0, 0, 1)). This treatment ensures a physically consistent representation of the polarization states in reduced dimensionality. In addition, within the 3D computational domain, the incident wave is configured to propagate in the x–z plane, which determines the definition of the polarization basis [14]. For s-polarized excitation, the electric field vector is constrained to the y-direction, E = (0, 1, 0), whereas p-polarized illumination is implemented by orienting the magnetic field along the same axis, H = (0, 1, 0). Fig. 3 illustrates in detail how the electromagnetic-field distributions of the two-dimensional and three-dimensional configurations of the gold grating are treated in COMSOL Multiphysics.

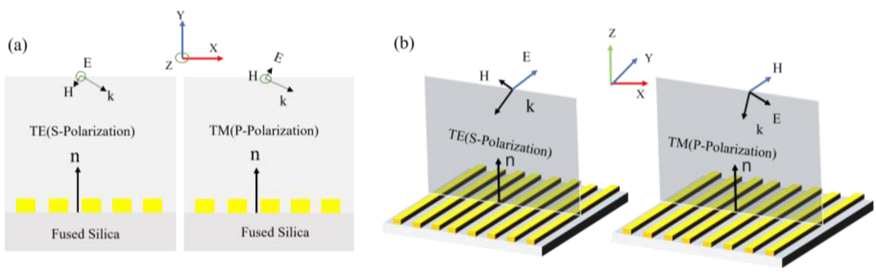

Figure 3. (a) 2D and (b) 3D representations of TE/TM polarization schemes in the grating model

The transient response was simulated using the Drude–Lorentz material model available in COMSOL Multiphysics. Floquet periodic boundary conditions were applied to model the patterned substrate as a single unit cell (Fig. 4(a)), where the fields on opposite boundaries are related through a complex phase factor defined by the transverse component of the incident wavevector. This treatment greatly reduces the computational cost [15]. A dense mesh was employed for spatial discretization (Fig. 4(b)) to accurately capture the geometrical features and ensure numerical robustness.

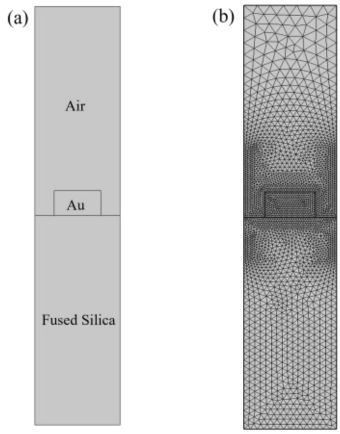

Figure 4. (a) Single unit-cell strcture of model and (b) mesh refinement of model

3. Results and discussion

To investigate the polarization response of the Au grating structures and evaluate the reliability of the numerical model, ellipsometric measurements were performed at multiple incident angles and compared with COMSOL simulations. Experimental characterization was performed using an M-2000 spectroscopic ellipsometer, and the measurement configuration is illustrated in Fig. 5. The light source generates a beam that is first linearly polarized by the polarizer, then the polarized beam impinges on the gold grating at an oblique incidence angle, where the interaction with the periodic metallic structure induces wavelength- and angle-dependent polarization changes. The reflected beam then passes through an analyzer that resolves the modified polarization state before reaching the detector [16]. By measuring the reflection-induced changes in amplitude and phase, the ellipsometric parameters Ψ and Δ are extracted. The two values (Ψ, Δ) express the amplitude ratio and phase difference p- and s-polarizations, respectively.

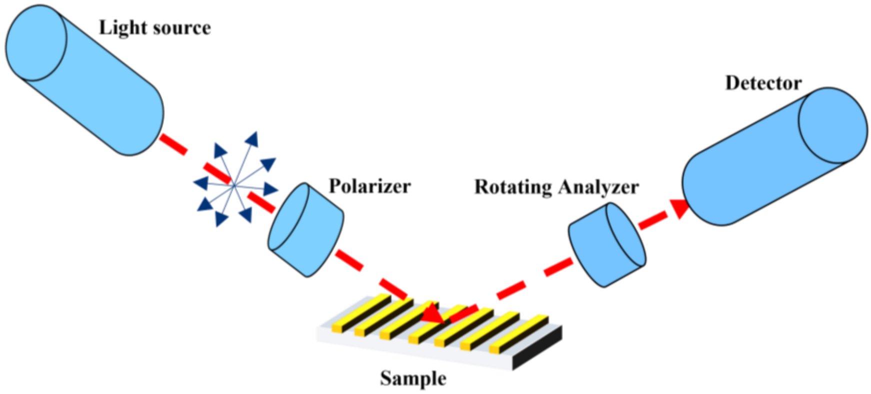

Figure 5. Schematic illustration of the M-2000 ellipsometry measurement on the gold grating

Figs. 6 and 7 show the measured and simulated Ψ and Δ spectra for critical dimensions (CD) of 70 nm and 110 nm, respectively. Overall, the experimental results exhibit a high level of consistency with the simulations, confirming that the geometric and material parameters used in the model are physically reasonable. Meanwhile, certain deviations between simulation and measurement are also observed, reflecting the sensitivity of the ellipsometric response to fabrication imperfections and optical material properties [17]. For the structure with CD= 70 nm, both simulated and experimental Ψ spectra display a pronounced resonance feature in the 450–600 nm wavelength region, which gradually shifts to longer wavelengths as the incident angle increases from 60° to 75°. This behavior indicates angle-dependent coupling of the incident light to guided modes or surface plasmon resonances supported by the subwavelength grating. Although the overall trend is consistent, the measured Ψ amplitude is slightly lower and exhibits smoother oscillations. These differences likely originate from surface roughness, and deviations in the optical constants of the deposited Au film relative to literature values, all of which tend to reduce the resonance strength. The Δ spectra exhibit a characteristic phase jump, particularly prominent around 600–750 nm. Both simulation and experiment capture this feature and its strong dependence on the incident angle, demonstrating that the grating effectively modulates the phase difference between p- and s-polarized components [18].

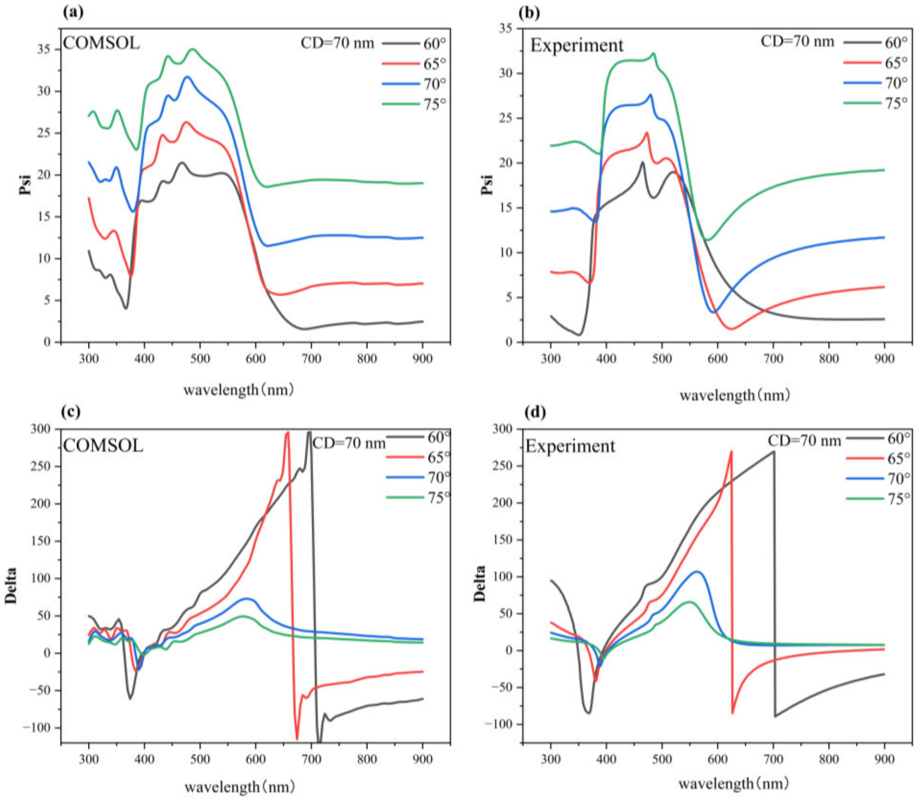

Figure 6. (a) and (b) show FEM simulated and measured Ψ spectra at Φ =60°; 65°; 70°; 75°,CD = 70 nm. (c) and (d) show FEM simulated and measured Δ spectra at Φ =60°; 65° ;70° ; 75°, CD= 70nm.

When the CD increases to 110 nm, the optical response undergoes a significant redshift. Both the simulation and experiment reveal that the main Ψ resonance now occurs in the 550–650 nm wavelength region, consistent with the expectation that larger grating features support longer-wavelength coupling conditions. With increasing incident angle, the Ψ peak gradually weakens and broadens, and this trend is consistently reproduced in both datasets. The experimental spectra show a slightly elevated baseline in the short-wavelength region (300–450 nm), which may be related to enhanced scattering and absorption originating from the actual surface morphology of the fabricated grating. And the Δ spectra for CD = 110 nm also show a pronounced phase jump, which shifts to longer wavelengths compared to the CD = 70 nm case. The simulated Δ exhibits a more abrupt transition, while the experimental transition is broadened and, at high incident angles, exhibits a slight blue shift. The discrepancy is reasonable considering that Δ is particularly sensitive to structural parameters such as grating depth, sidewall slope, and Au dispersion. Even a few nanometers of deviation in the grating cross-section can measurably influence the phase response, leading to the observed experimental variations[19].

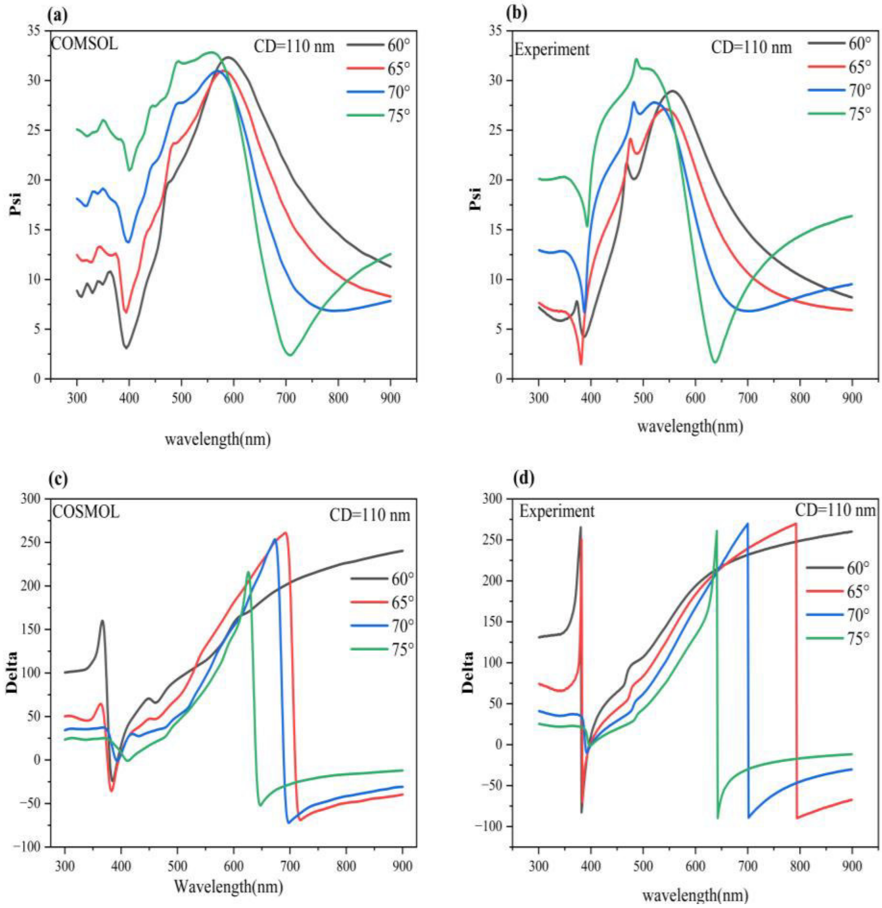

Figure 7. (a) and (b) show FEM simulated and measured Ψ spectra at Φ =60°; 65° ; 70° ; 75°, CD= 110nm. (c) and (d) show FEM simulated and measured Δ spectra at Φ =60°; 65° ;70° ;75° , CD= 110nm.

The near-field distributions (Fig. 8) under s- and p-polarized excitation exhibit fundamentally distinct behaviors arising from the different boundary conditions imposed at the metal–dielectric interface. Under TE (s-polarization) illumination, the electric field remains weakly confined and predominantly distributed within the dielectric region above the grating, forming smooth interference fringes characteristic of diffractive propagation without significant surface coupling [20]. In contrast, TM (p-polarization) excitation generates pronounced field localization at the metal ridge edges and along the grating sidewalls, where the electric-field component normal to the interface efficiently drives charge oscillations and enables strong coupling to plasmonic-like or guided-mode resonances. This results in sharply confined hotspots with substantially higher $|E|^2$ amplitude and rapid evanescent decay away from the surface. The markedly stronger confinement and resonance-induced enhancement observed for TM illumination directly correlate with the sharper spectral features and phase transitions in the corresponding ellipsometric Ψ and Δ responses, confirming that the dominant optical sensitivity of the grating arises from TE-driven and TM-driven surface-field interactions.

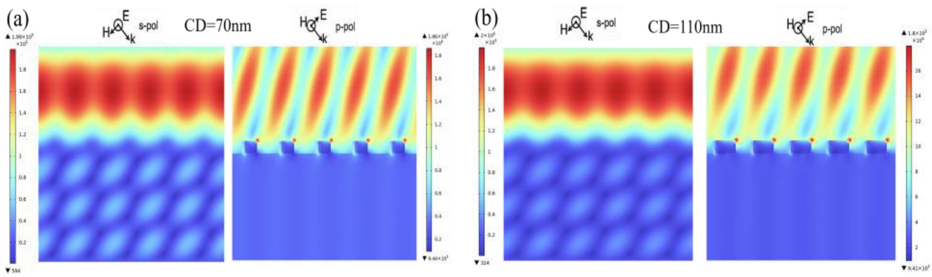

Figure 8. (a) and (b) show the electric field distribution(V/m) maps for TE (s-pol) and TM (p-pol) waves, respectively, extracted for an incident wavelength of 380 nm, for structures with CD values of 70 nm and 110 nm.

4. Conclusions

The validated simulation–experiment workflow confirms that numerical ellipsometry can be reliably applied to guide the design of high-sensitivity plasmonic components. By accurately predicting spectral shifts, resonance strengths, and phase transitions associated with TM-dominant field localization, the method enables rational optimization of grating dimensions, dispersion models, and material choices. These results position the approach as a practical tool for developing next-generation photonic systems including surface-enhanced sensors, integrated optical modulators, and nanoscale spectral filters with improved performance and fabrication tolerance.

Acknowledgements

Support from projects OTKA K-146181, and 20FUN02 POLight are acknowledged. The TKP2021-EGA04 project have been implemented with support from the Ministry of Innovation and Technology of Hungary from the National Research, Development and Innovation Fund.

References

[1] M. Moharam and T. K. Gaylord, "Rigorous coupled-wave analysis of planar-grating diffraction," *Journal of the Optical Society of America,* vol. 71, no. 7, pp. 811-818, 1981.

[2] L. Li, "Formulation and comparison of two recursive matrix algorithms for modeling layered diffraction gratings," *Journal of the Optical Society of America A,* vol. 13, no. 5, pp. 1024-1035, 1996.

[3] N. K. Pavlycheva, "Diffraction gratings for spectral devices," *Journal of Optical Technology,* vol. 89, no. 3, pp. 142-150, 2022.

[4] T. W. Ebbesen, H. J. Lezec, H. Ghaemi, T. Thio, and P. A. Wolff, "Extraordinary optical transmission through sub-wavelength hole arrays," *Nature,* vol. 391, no. 6668, pp. 667-669, 1998.

[5] W. L. Barnes, A. Dereux, and T. W. Ebbesen, "Surface plasmon subwavelength optics," *nature,* vol. 424, no. 6950, pp. 824-830, 2003.

[6] F. Hong and R. Blaikie, "Plasmonic lithography: recent progress," *Advanced Optical Materials,* vol. 7, no. 14, p. 1801653, 2019.

[7] W.-L. Yeh, C.-M. Fang, and Y.-P. Chiou, "Enhancing LED light extraction by optimizing cavity and waveguide modes in grating structures," *Journal of Display Technology,* vol. 9, no. 5, pp. 359-364, 2013.

[8] R. Messina, A. Noto, B. Guizal, and M. Antezza, "Radiative heat transfer between metallic gratings using Fourier modal method with adaptive spatial resolution," *Physical Review B,* vol. 95, no. 12, p. 125404, 2017.

[9] D. Mukherjee, S. Burger, T. Siefke, J. Gour, B. Bodermann, and P. Petrik, "Spectroscopic Ellipsometry of Plasmonic Gratings─ Ideal Parameters for Sensing and Subpicometer Measurement Uncertainty," *ACS Omega,* vol. 10, no. 14, pp. 14466-14473, 2025.

[10] M. Li, S. K. Cushing, and N. Wu, "Plasmon-enhanced optical sensors: a review," *Analyst,* vol. 140, no. 2, pp. 386-406, 2015.

[11] D. Mukherjee *et al.*, "Optimized sensing on gold nanoparticles created by graded-layer magnetron sputtering and annealing," *Sensors and Actuators B: Chemical,* vol. 425, p. 136875, 2025.

[12] R. Hiramatsu *et al.*, "Three-Method Hybrid Numerical Simulation for Surface-Plasmon-Enhanced GaInN-Based Light-Emitting Diodes with Metal-Embedded Nanostructures," *Frontiers in Physics,* vol. 9, p. 710092, 2021.

[13] E. Hirose, D. Sakai, A. Iida, Y. Obayashi, and J. Nishikawa, "Exumbrellar surface of jellyfish: a comparative fine structure study with remarks on surface reflectance," *Zoological Science,* vol. 38, no. 2, pp. 170-178, 2021.

[14] U. Hohenester and A. Trügler, "MNPBEM–A Matlab toolbox for the simulation of plasmonic nanoparticles," *Computer Physics Communications,* vol. 183, no. 2, pp. 370-381, 2012.

[15] N. M. Lyndin, O. Parriaux, and A. V. Tishchenko, "Modal analysis and suppression of the Fourier modal method instabilities in highly conductive gratings," *Journal of the Optical Society of America A,* vol.

24, no. 12, pp. 3781-3788, 2007.

[16] V. G. Kravets, A. V. Kabashin, W. L. Barnes, and A. N. Grigorenko, "Plasmonic surface lattice resonances: a review of properties and applications," *Chemical Reviews,* vol. 118, no. 12, pp. 5912-5951, 2018.

[17] P. Urbancova, J. Chylek, P. Hlubina, and D. Pudis, "Guided-mode resonance-based relative humidity sensing employing a planar waveguide structure," *Sensors,* vol. 20, no. 23, p. 6788, 2020.

[18] M. Kashif, A. A. A. Bakar, N. Arsad, and S. Shaari, "Development of phase detection schemes based on surface plasmon resonance using interferometry," *Sensors,* vol. 14, no. 9, pp. 15914-15938, 2014.

[19] H. Gross, S. Heidenreich, and M. Bär, "Impact of different stochastic line edge roughness patterns on measurements in scatterometry-a simulation study," *Measurement,* vol. 98, pp. 339-346, 2017.

[20] A. Sierant, B. R. Jany, and T. Kawalec, "Near-field characterization of surface plasmon polaritons on a nanofabricated transmission structure," *Physical Review B,* vol. 103, no. 16, p. 165433, 2021.